Supporting Information

Tunable NIR AIE-active optical materials for lipid droplets imaging in typical model organism and photodynamic therapy

Fei Zhang, [a] Yaoming Liu, [b] Binsheng Yang, [a] Pengli Guan, [a] Jie Chai, [c] Guangming Wen [c] and Bin Liu*[a]

[a]*Institute of Molecular Science, Engineering Research Center for Sewage Treatment of Shanxi Province, Shanxi University, Taiyuan, China, 030006. E-mail: liubin@sxu.edu.cn.*

[b]*Scientific Instrument Center of Shanxi University, Taiyuan, China.*

[c]*Department of Chemistry, Jinzhong University, Jinzhong, 030619, China.*

Contents

1. Experimental section

2. Characterization of compounds

3. **Particle size distributions**

4. PL spectra in various solvents.

5. Cyclic voltammetric curves.

6. Cell imaging

7. Photostability analysis

8. Colocalization imaging of *Locusta migratoria* corpus adiposum

9. Colocalization imaging of *Caenorhabditis elegans*

10. Colocalization imaging of zebrafish

11. Colocalization imaging of sunflower

Table S1. Crystal data and structure refinement of TPTIs

Table S2. Data of bandgaps of theoretical study and cyclic voltammetry

Table S3. Photophysical properties of LDs probes and their applications

1. Experimental section

1.1. Materials and methods

All chemical materials and organic solvents were commercially available and used without any purification. 4-Bromo-N, N-diphenylaniline, (4-formylphenyl) boronic acid, (5-bromofuran-2-yl) boronic acid, (5-bromothiophen-2-yl) boronic acid, 3,5,5-trimethylcyclohex-2-en-1-one, malononitrile and [1,1′-Bis(diphenylphosphino)ferrocene] dichloropalladium were purchased from Aladdin. The product was purified by chromatography on silica gel (300–400 mesh). Buffer solution (PBS 1×, pH 7.4) was prepared with distilled water. ^{1}H NMR, ^{13}C NMR spectra were recorded on a Bruker Avance III-600MHz spectrometers. The chemical shift of NMR spectrum was expressed in ppm, relative to the internal standard of TMS (^{1}H, 0.00 ppm). High resolution mass spectra were acquired using a Thermo Scientific Q Exactive LC-MS spectrometer. UV-vis spectra were recorded on a Hitachi 5300 absorption spectrophotometer. Fluorescence spectra were recorded on a Varian Cary Eclipse fluorescence spectrophotometer. Cyclic voltammetric measurements were carried out on a computer-controlled CHI 660C instrument. Absolute fluorescence quantum yield and decay time was measured on FLS980 (Edinburgh Instruments). Cell imaging and *in vivo* imaging were performed by using a confocal laser scanning microscope (Zeiss LSM-880). Density functional theory (DFT) calculations using the B3LYP functional were conducted with the Gaussian 09 software package. Dynamic light scatting (DLS) experiments were conducted with ALV5000 Laser Light Scattering Instrument.

1.2. Synthesis

1.2.1. Synthesis of 2-(3,5,5-trimethylcyclohex-2-en-1-ylidene) malononitrile

The intermediates of 2-(3,5,5-trimethylcyclohex-2-en-1-ylidene) malononitrile was synthesized following the literature procedure.[1] ^{1}H NMR (600 MHz, $CDCl_3$): 6.62–6.63 (m, 1H), 2.52 (s, 2H), 2.18 (s, 2H), 2.041–2.042 (d, J = 0.9 Hz, 3H), 1.02 (s, 6H).

*1.2.2. Synthesis of **TPB***

A mixture of 4-bromo-N,N-diphenylaniline (323 mg, 1.00 mmol), potassium carbonate (1.18 g, 10.0 mmol), (4-formylphenyl)boronic acid (0.150 g, 1.00 mmol) and [1,1′-Bis(diphenylphosphino) ferrocene]dichloropalladium (7.00 mg, 1 mol%) were dissolved in 10 mL of isopropyl alcohol with deionized water (10 mL) in a 50 mL three-neck bottle with a

magnetic stirring bar under nitrogen atmosphere. The reaction mixture was stirred at 100 °C for 2 h, then cooled to room temperature and the solvent was removed under vacuum. Deionized water (100 mL) was added to crude product and then extracted with ethyl acetate (30 mL × 3). The obtained yellow extraction was dried with Na_2SO_4, and then the solvent was evaporated. The crude solid product was purified by column chromatography ($V_{petroleum\ ether}$: $V_{CH_2Cl_2}$, 1:1). The final product was yellow powdery solid (0.320 g, 92%). ^{1}H NMR (600 MHz, $CDCl_3$): 10.05 (s, 1H), 7.95 (d, *J* = 8.04 Hz, 2H), 7.76 (d, *J* = 8.10 Hz, 2H), 7.55 (d, *J* = 8.54 Hz, 2H), 7.32 (t, *J* = 7.64 Hz, 4H), 7.18 (d, *J* = 2.69 Hz, 3H), 7.17 (d, *J* = 3.07 Hz, 3H), 7.10 (t, *J* = 7.32 Hz, 2H).

1.2.3. Synthesis of ***TPF***

The synthetic procedure was the same as that of **TPB**. The obtained product was yellow oily liquid (0.820 g, 80%). ^{1}H NMR (600 MHz, $CDCl_3$): 9.61 (s, 1H), 7.69 (t, *J* = 8.98 Hz, 1H), 7.67 (t, *J* = 2.18 Hz, 1H), 7.33 (t, *J* = 2.04 Hz, 1H), 7.32 (d, *J* = 1.10 Hz, 3H), 7.30 (t, *J* = 2.04 Hz, 1H), 7.17 (d, *J* = 1.09 Hz, 2H), 7.16 (d, *J* = 1.09 Hz, 2H), 7.13 (t, *J* = 1.04 Hz, 1H), 7.12 (d, *J* = 1.09 Hz, 1H), 7.11 (d, *J* = 1.46 Hz, 2H), 7.09 (t, *J* = 2.08 Hz, 1H).

1.2.4. Synthesis of ***TPT***

The synthetic procedure was the same as that of **TPF**, and the obtained product was yellow solid (0.120 g, 34%). ^{1}H NMR (600 MHz, $CDCl_3$): 9.88 (s, 1H), 7.73 (d, *J* = 3.89 Hz, 1H), 7.55 (t, *J* = 1.95 Hz, 1H), 7.53 (t, *J* = 1.95 Hz, 1H), 7.33 (d, *J* = 2.00 Hz, 1H), 7.32 (d, *J* = 1.15 Hz, 3H), 7.31 (d, *J* = 1.92 Hz, 1H), 7.17 (d, *J* = 1.04 Hz, 2H), 7.15 (d, *J* = 0.96 Hz, 2H), 7.11 (t, *J* = 0.81 Hz, 1H), 7.09 (t, *J* = 2.15 Hz, 3H).

1.2.5. Synthesis of ***TPBIs***

A solution of **TPB** (0.349 g, 1.00 mmol) and 2-(3,5,5-trimethylcyclohex-2-en-1-ylidene) malononitrile (0.186 g, 1.00 mmol) were refluxed in dry acetonitrile with a drop of piperidine as catalyst for 2 h, then cooled to room temperature. The mixture was filtered and the product was obtained as red solid (0.185 g, 36%). ^{1}H NMR (600 MHz, $CDCl_3$) (Fig. S1): 7.64 (d, *J* = 5.84 Hz 2H), 7.58 (d, *J* = 5.16 Hz, 2H), 7.52 (d, *J* = 6.54 Hz, 2H), 7.30 (d, *J* = 7.93 Hz, 4H), 7.28 (t, *J* = 3.32 Hz, 2H), 7.16 (t, *J* = 3.48 Hz, 4H), 7.09 (d, *J* = 10.38 Hz, 2H), 7.06 (s, 1H), 7.03 (s, 1H), 6.88 (s, 1H), 2.63 (s, 2H), 2.51 (s, 2H), 1.11 (s, 6H). ^{13}C NMR (150 MHz, $CDCl_3$) (Fig. S2): 169.22, 153.93, 147.82, 147.48, 141.94, 136.75, 134.07, 133.49, 129.36, 128.74, 128.13, 127.59, 126.98, 124.68, 124.57, 123.49, 123.25, 113.59, 112.82, 43.03, 39.25,

32.07, 28.06. ESI mass spectrometry (Fig. S3): m/z = 518.2585 $[M+H]^+$, $[M+H]^+$ calculated 518.2591.

*1.2.6. Synthesis of **TPFIs***

The synthetic procedure was the same as that of **TPBIs**. The product was obtained as black solid (0.150 g, 30%). ^{1}H NMR (600 MHz, $CDCl_3$) (Fig. S4): 7.61 (d, J = 7.38 Hz, 2H), 7.31 (d, J = 4.92 Hz, 3H), 7.28 (t, J = 1.68 Hz, 2H), 7.16 (d, J = 6.12 Hz, 4H), 7.10 (t, J = 6.06 Hz, 4H), 6.94 (d, J = 8.12 Hz, 1H), 6.86 (s, 1H), 6.65 (s, 2H), 2.60 (s, 2H), 2.43 (s, 2H), 1.09 (s, 6H). ^{13}C NMR (150 MHz, $CDCl_3$) (Fig. S5): 168.83, 154.97, 153.67, 148.26, 147.38, 147.28, 147.17, 146.60, 139.81, 133.52, 131.51, 130.13, 129.51, 129.44, 129.41, 128.27, 127.73, 127.26, 127.04, 126.78, 126.68, 126.52, 124.94, 124.85, 123.61, 123.17, 122.91, 122.85, 113.03, 76.83, 42.94, 39.15, 32.02, 28.04, 27.81. ESI mass spectrometry (Fig. S6): m/z = 508.2377 $[M+H]^+$, $[M+H]^+$ calculated 508.2383.

*1.2.7. Synthesis of **TPTIs***

The synthetic process was the same as that of **TPFIs**, and the obtained product was black solid (0.200 g, 38%). ^{1}H NMR (600 MHz, $CDCl_3$) (Fig. S7): 7.48 (d, J = 4.14 Hz, 2H), 7.30 (d, J = 4.92 Hz, 3H), 7.28 (d, J = 8.80 Hz, 3H), 7.19 (s, 1H), 7.16 (d, J = 8.80 Hz, 5H), 7.09 (d, J = 7.62 Hz, 4H), 6.81 (s, 1H), 2.60 (s, 2H), 2.44 (s, 2H), 1.09 (s, 6H). ^{13}C NMR (150 MHz, $CDCl_3$) (Fig. S8): 168.56, 155.52, 154.27, 147.53, 147.42, 147.39, 147.28, 146.20, 138.27, 135.76, 134.23, 133.33, 130.35, 128.36, 128.55, 127.36, 126.33, 126.13, 125.33, 125.14, 125.04, 124.38, 123.67, 122.80, 122.52, 122.03, 121.03, 120.35, 115.05, 76.22, 43.25, 40.15, 33.05, 28.28, 27.35. ESI mass spectrometry (Fig. S9): m/z = 524.2145 $[M+H]^+$, $[M+H]^+$ calculated 524.2155.

1.3. Cell culture

The human liver cancer cells line SMMC-7721 and PC12 cells were supplied by the cell resource center of Chinese academy sciences. They were cultured at 37 °C and 5% CO_2 incubator in RPMI-1640 medium containing 10% fetal bovine serum (FBS) and 1% penicillin-streptomycin (10^4 U•mL^{-1} penicillin and 10^4 μg•mL^{-1} streptomycin).

2. Characterization of compounds

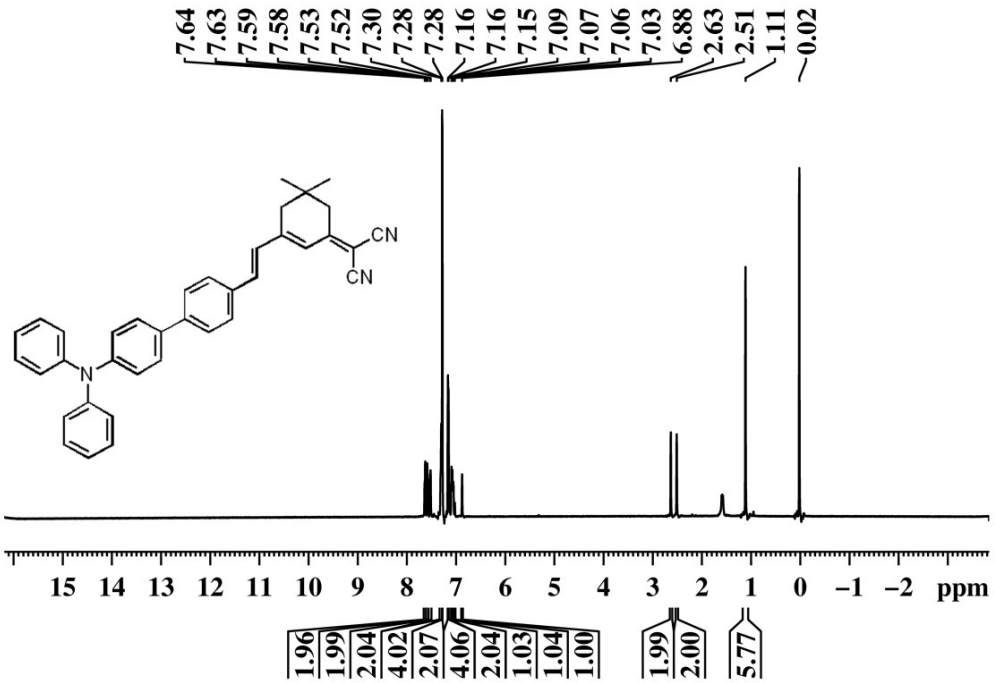

Fig. S1 ^{1}H NMR of **TPBIs** in $CDCl_3$.

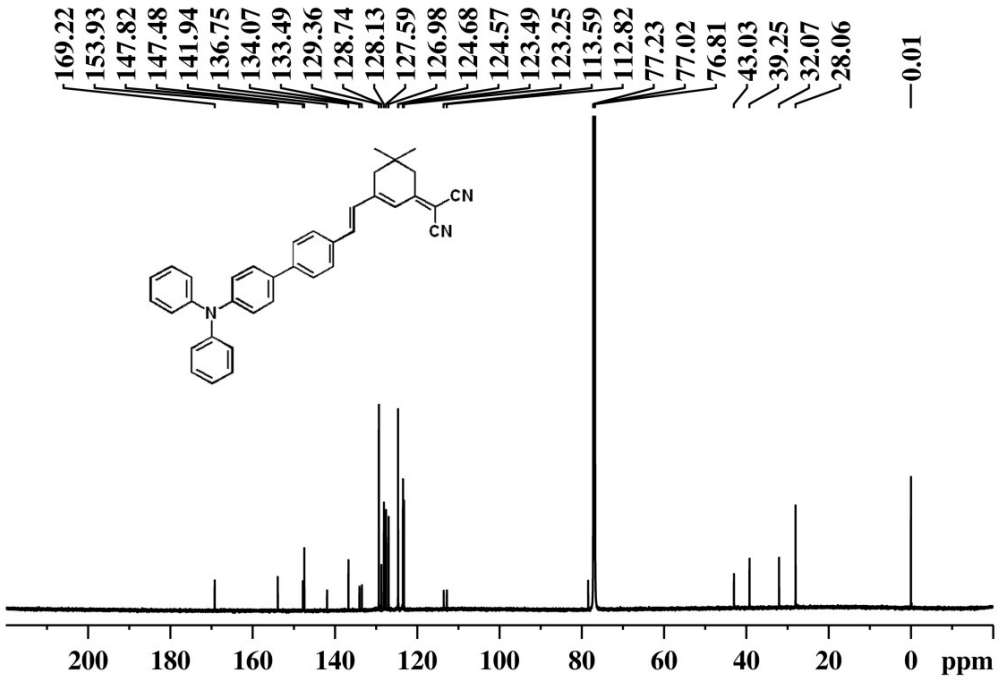

Fig. S2 ^{13}C NMR of **TPBIs** in $CDCl_3$.

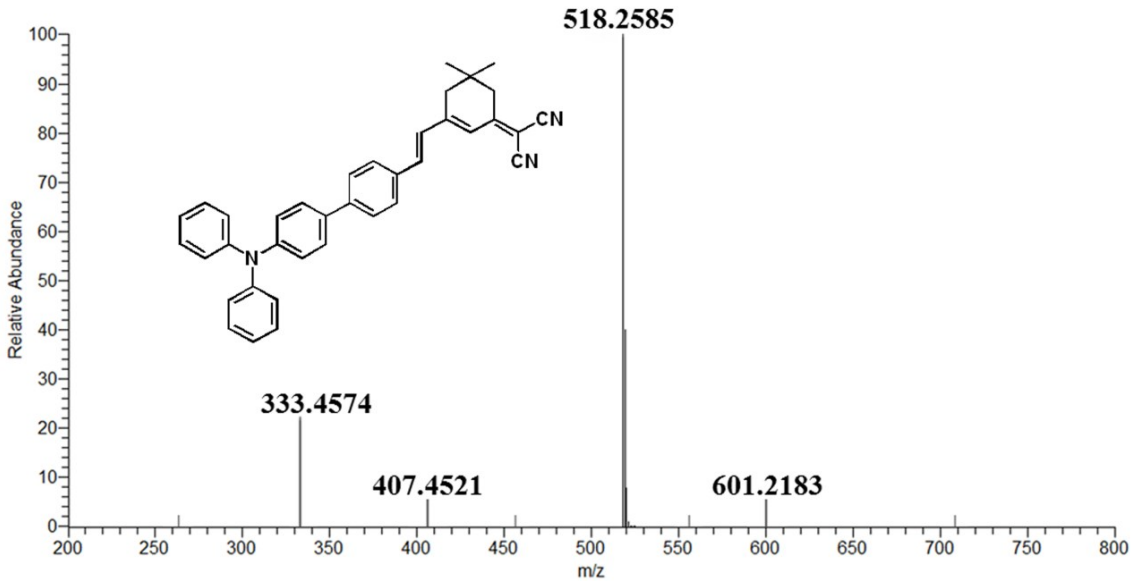

Fig. S3 ESI-MS spectrum of **TPBIs.**

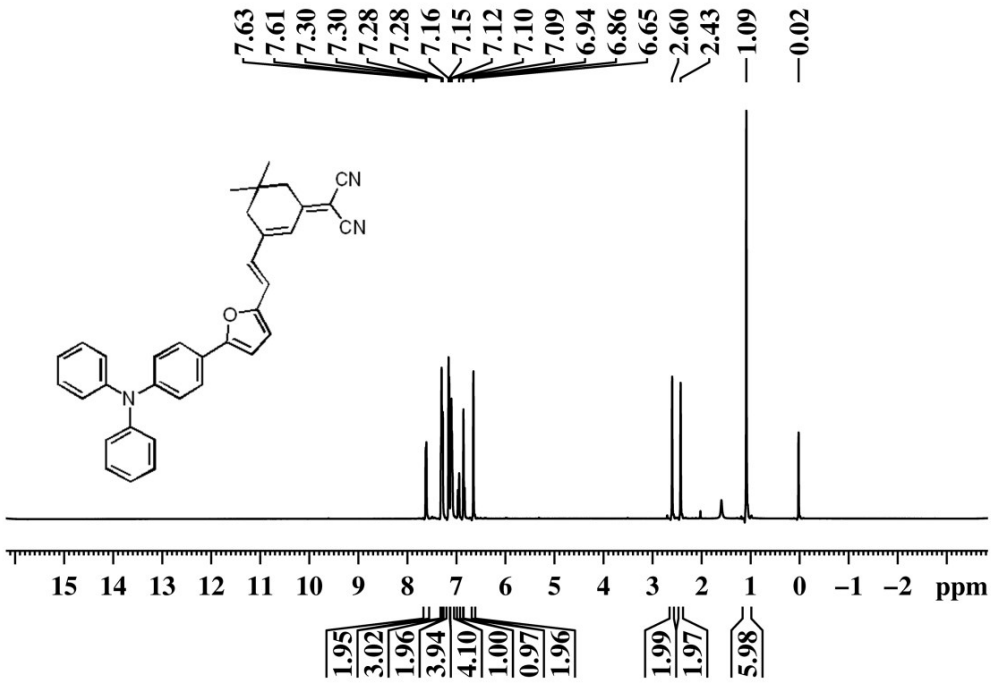

Fig. S4 ^{1}H NMR of **TPFIs** in $CDCl_3$.

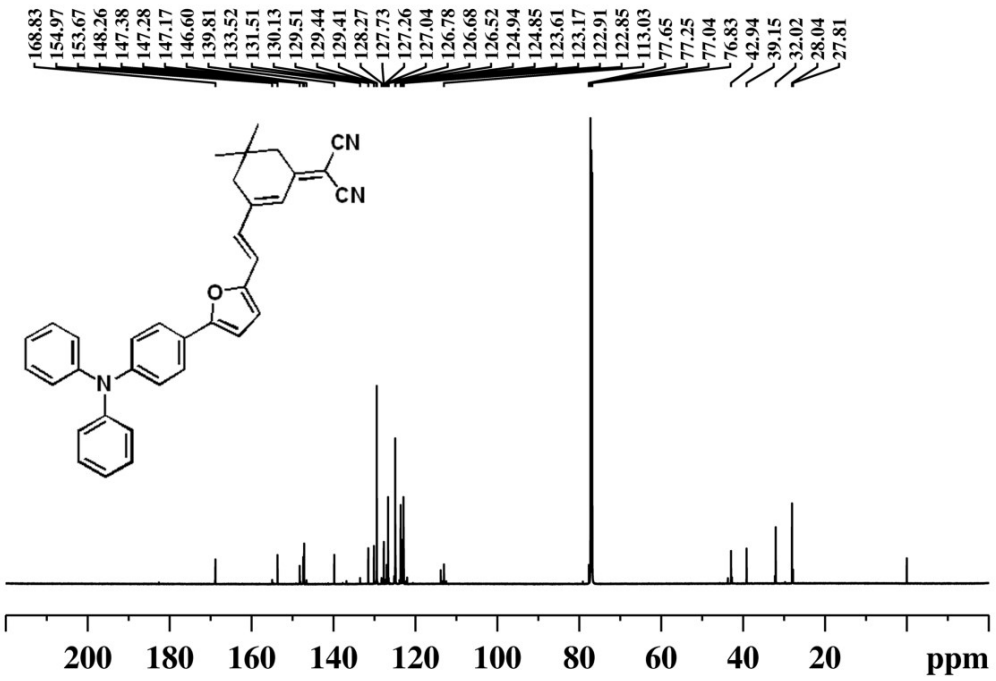

Fig. S5 ^{13}C NMR of **TPFIs** in $CDCl_3$.

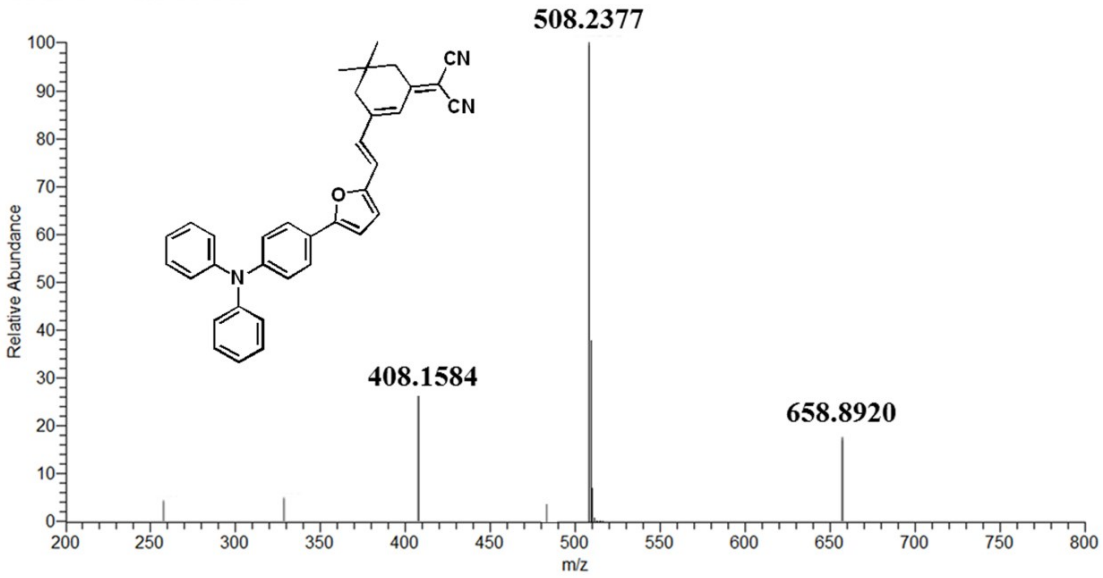

Fig. S6 ESI-MS spectrum of **TPFIs.**

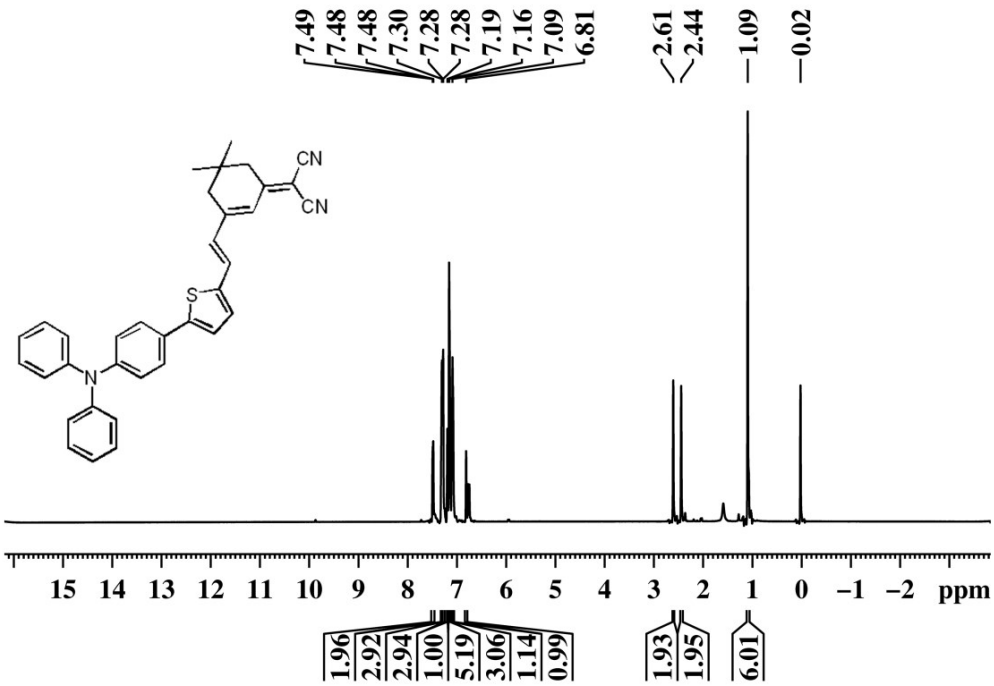

Fig. S7 ^{1}H NMR of **TPTIs** in $CDCl_3$.

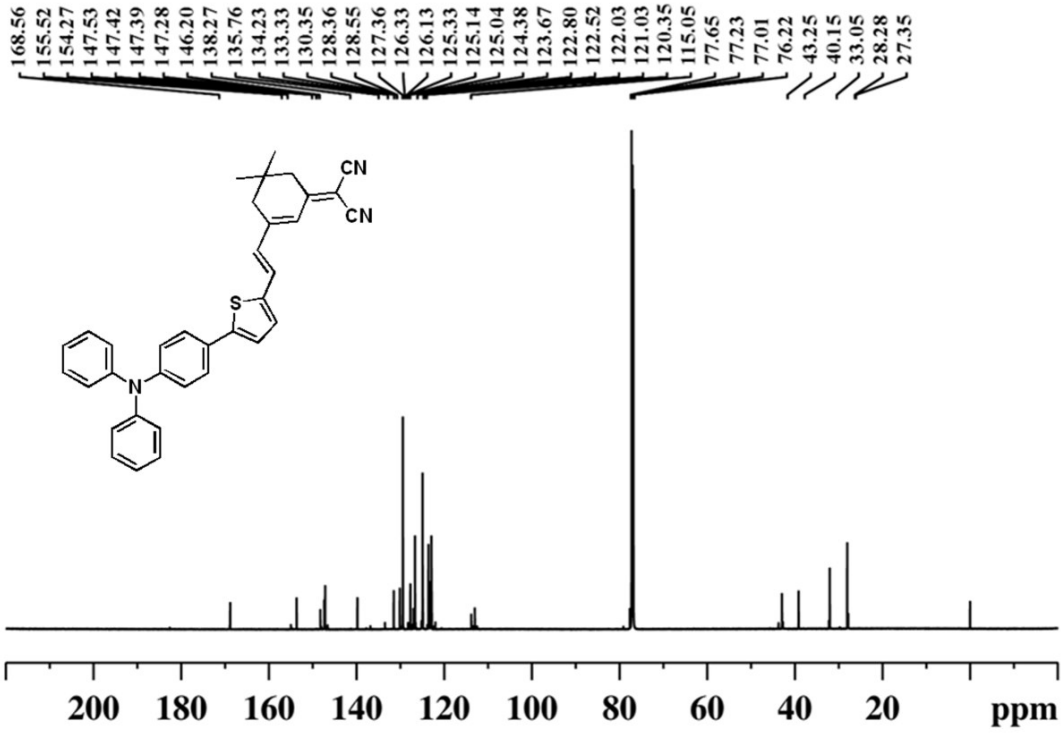

Fig. S8 ^{13}C NMR of **TPTIs** in $CDCl_3$.

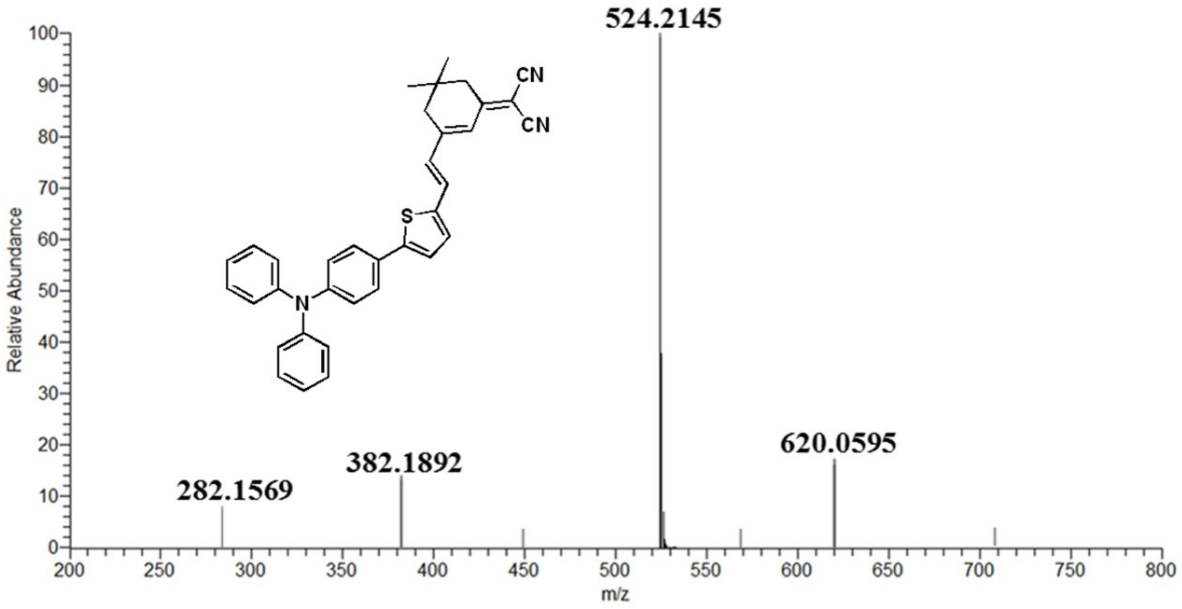

Fig. S9 ESI-MS spectrum of **TPTIs.**

3. Particle size distributions

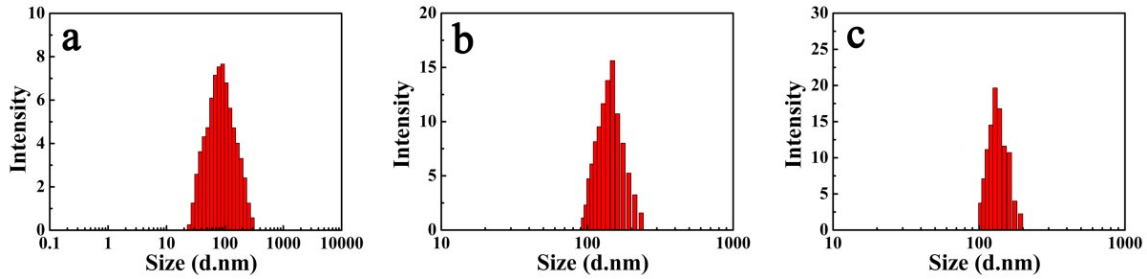

Fig. S10 Particle size distributions of **TPBIs** (a), **TPFIs** (b) and **TPTIs** (c) in toluene. Concentration: 10 μM.

4. PL spectra in various solvents.

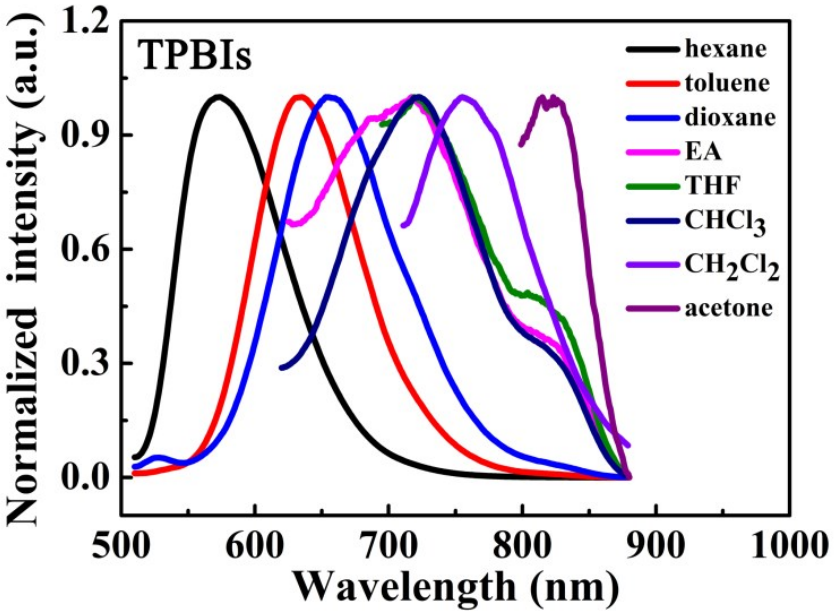

Fig. S11 Normalized PL spectra of **TPBIs** in various solvents.

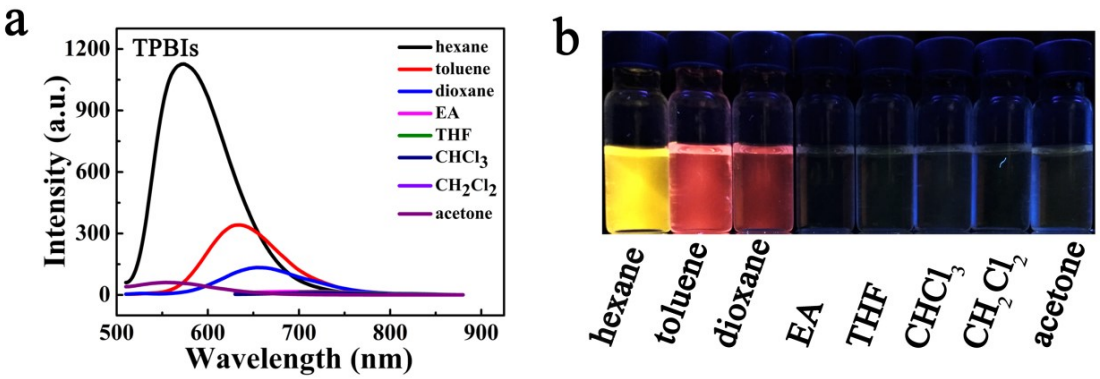

Fig. S12 a) PL spectra of **TPBIs** in various solvents. Concentration: 1.0 μM; excitation wavelength: 494 nm. b) Photographs: showing the solution under UV light.

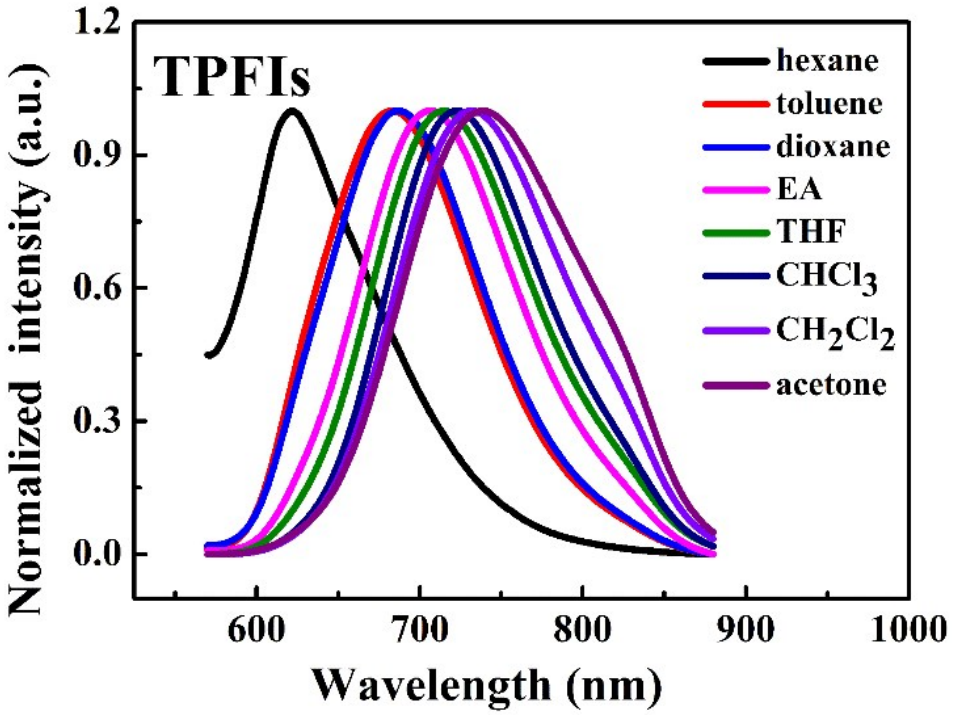

Fig. S13 Normalized PL spectra of **TPFIs** in various solvents.

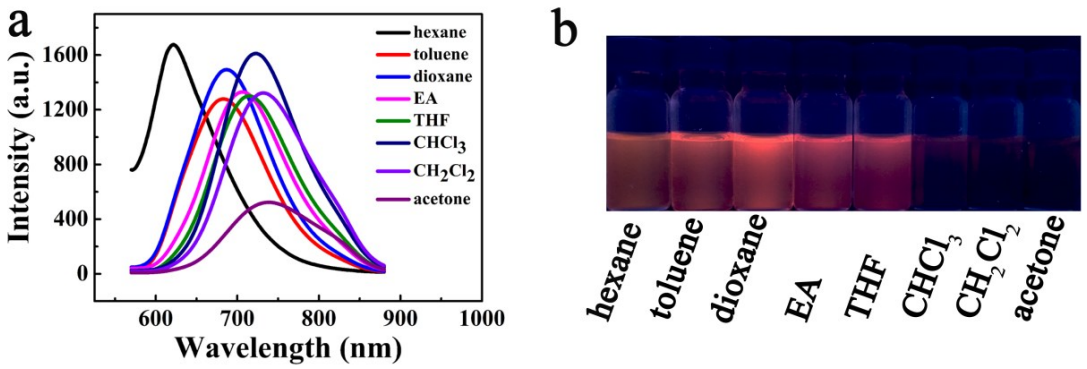

Fig. S14 a) PL spectra of **TPFIs** in various solvents. Concentration: 1.0 μM; excitation wavelength: 549 nm. b) Photographs: showing the solution under UV light.

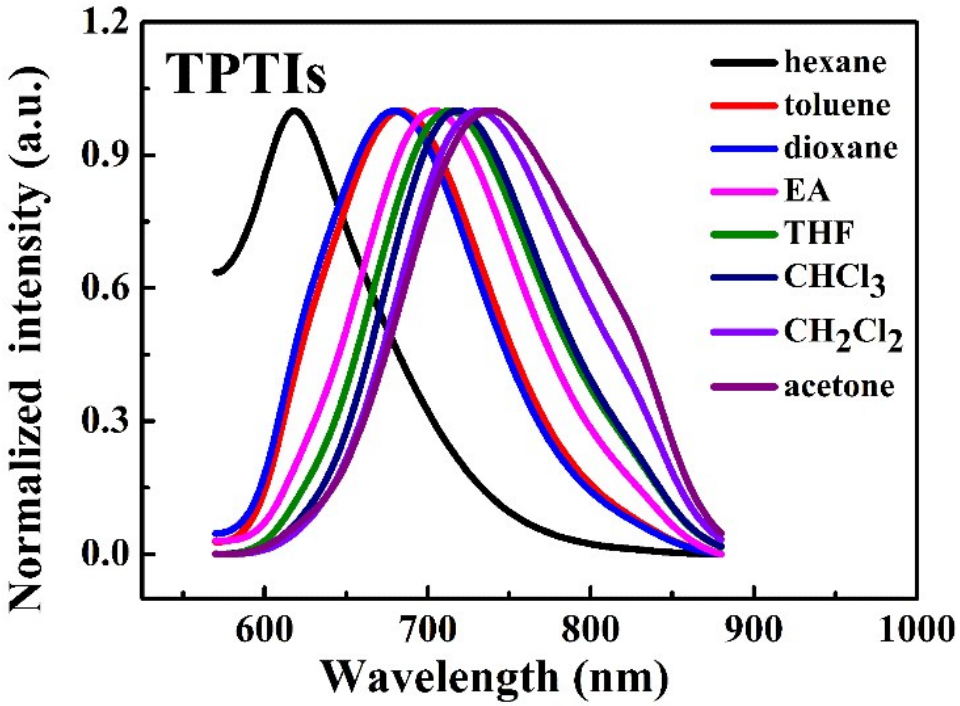

Fig. S15 Normalized PL spectra of **TPTIs** in various solvents.

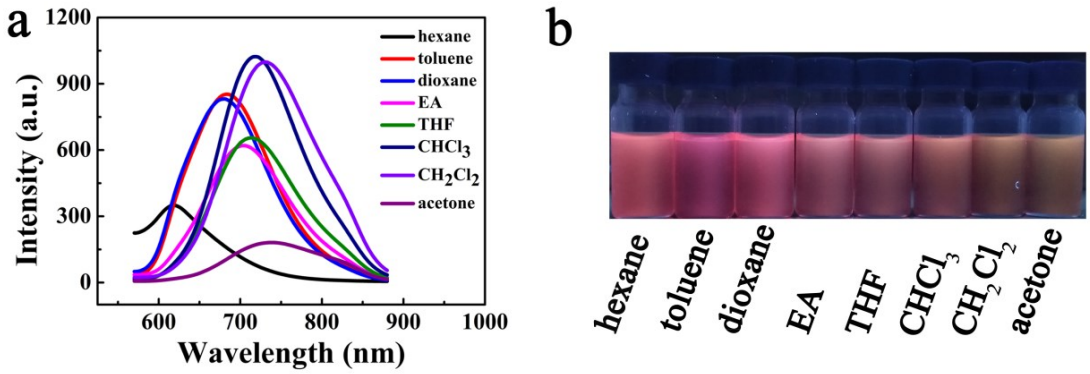

Fig. S16 a) PL spectra of **TPTIs** in various solvents. Concentration: 1 μM; excitation wavelength: 547 nm. b) Photographs: showing the solution under UV light.

5. Cyclic voltammetric curves.

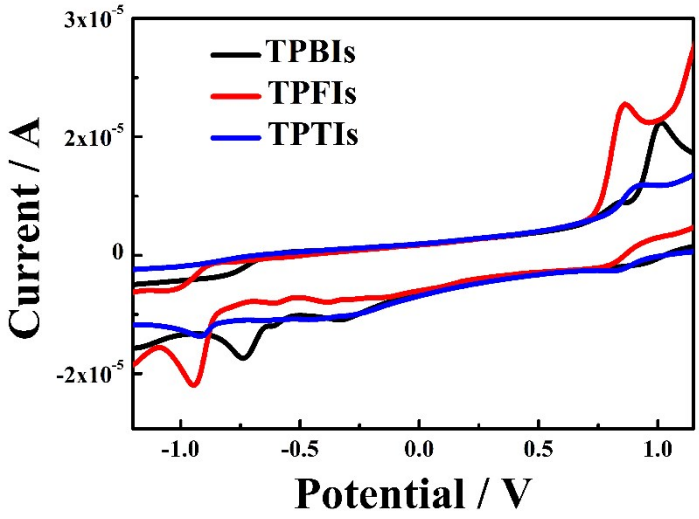

Fig. S17 Cyclic voltammetric curves of **TPBIs**, **TPFIs** and **TPTIs** in acetonitrile. Concentration: 100 μM.

6. Cell imaging

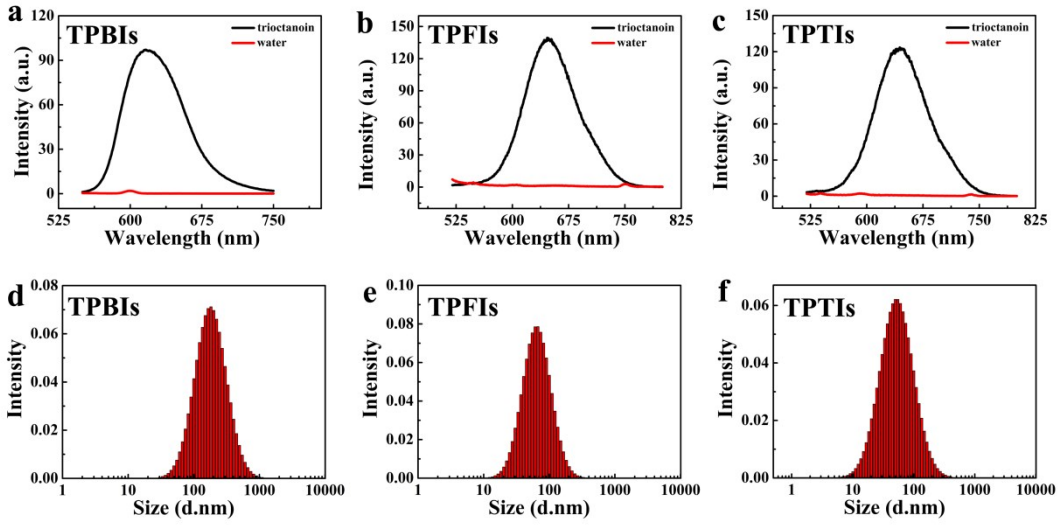

Fig. S18 PL spectra of **TPBIs** (a), **TPFIs** (b) and **TPTIs** (c) in trioctanoin and water. Concentration: 1.0 μM; excitation wavelength: 488 nm. b) Particle size distributions of **TPBIs** (d), **TPFIs** (e) and **TPTIs** (f) in aqueous solution with 1 % DMSO. Concentration: 1.0 μM.

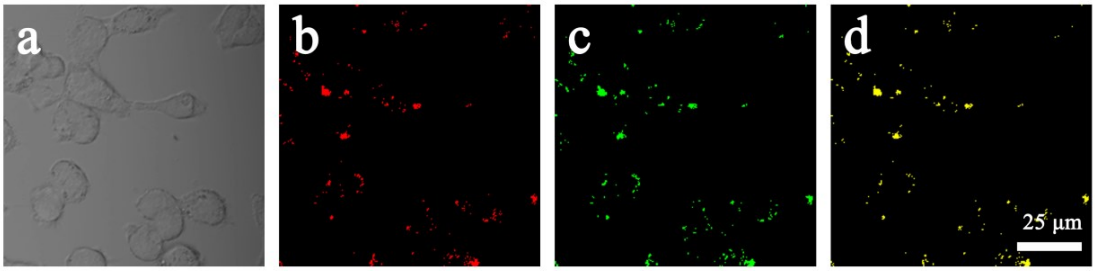

Fig. S19 Colocalization imaging of PC12 incubated with **TPFIs** and BODIPY493/503 Green. a) Bright-field, b) red channel and c) green channel. d) merged images of panels (b) and (c). For **TPFIs**, λ_{ex}= 488 nm, λ_{em}= 600–750 nm; For BODIPY 493/503, λ_{ex}= 488 nm, λ_{em}= 500–570 nm. Concentrations: **TPFIs** (1×10^{-6} M), BODIPY493/503 Green (1.0×10^{-6} M).

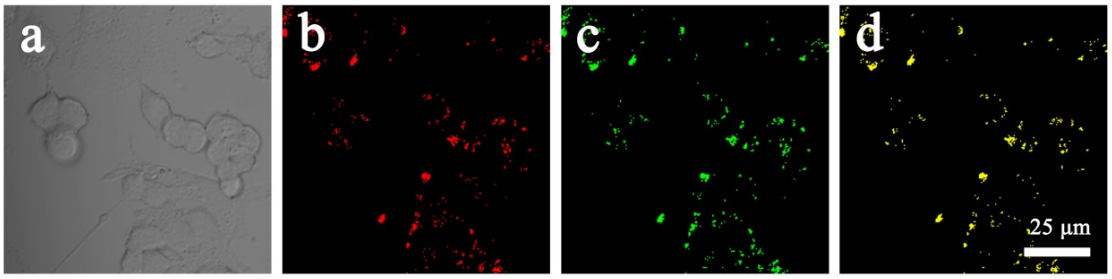

Fig. S20 Colocalization imaging of PC12 incubated with **TPTIs** and BODIPY493/503 Green. a) Bright-field, b) red channel and c) green channel. d) merged images of panels (b) and (c). For **TPTIs**, λ_{ex}= 488 nm, λ_{em}= 600–750 nm; For BODIPY 493/503, λ_{ex}= 488 nm, λ_{em}= 500–570 nm. Concentrations: **TPTIs** (1×10^{-6} M), BODIPY493/503 Green (1.0×10^{-6} M).

7. Photostability analysis

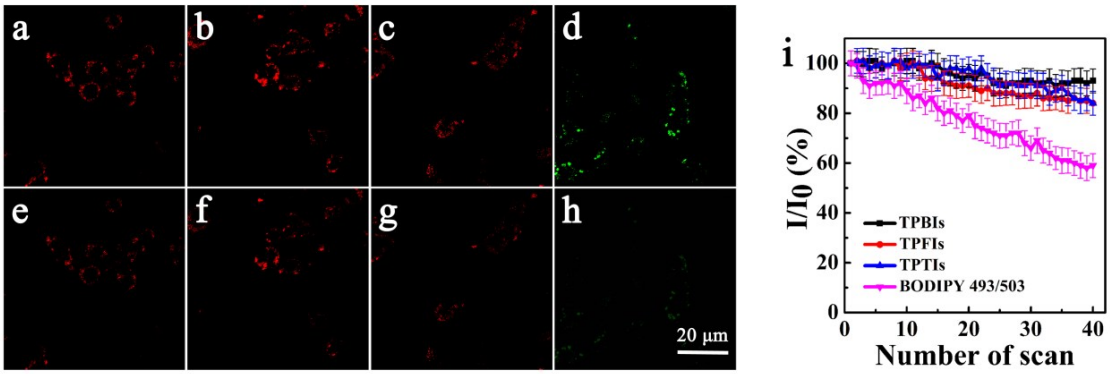

Fig. S21 Confocal images of PC12 cells a–d) before and e–h) after the laser irradiation for 15 min stained with a, e) **TPBIs**, b, f) **TPFIs**, c, g) **TPTIs**, and d, h) BODIPY493/503 Green i) Loss of fluorescence in PC12 cells stained with AIEgens and BODIPY493/503 Green. Concentration: 0.1 μM (**TPBIs**, **TPFIs**, and **TPTIs**) and 0.2 μM (BODIPY493/503 Green). λ_{ex}: 488 nm, laser power of confocal fluorescence microscope: 0.5 μW.

8. Colocalization imaging of *Locusta migratoria* corpus adiposum

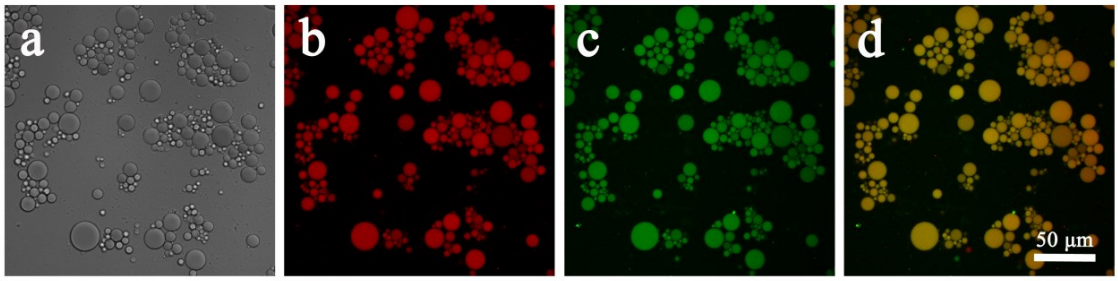

Fig. S22 Colocalization imaging of *Locusta migratoria* corpus adiposum incubated with **TPFIs** and BODIPY493/503 Green. a) Bright-field, b) red channel and c) green channel. d) merged images of panels (b) and (c). For **TPFIs**, λ_{ex}= 488 nm, λ_{em}= 600–750 nm; For BODIPY 493/503, λ_{ex}= 488 nm, λ_{em}= 500–570 nm. Concentrations: **TPFIs** (1.0×10^{-6} M), BODIPY493/503 Green (1×10^{-6} M).

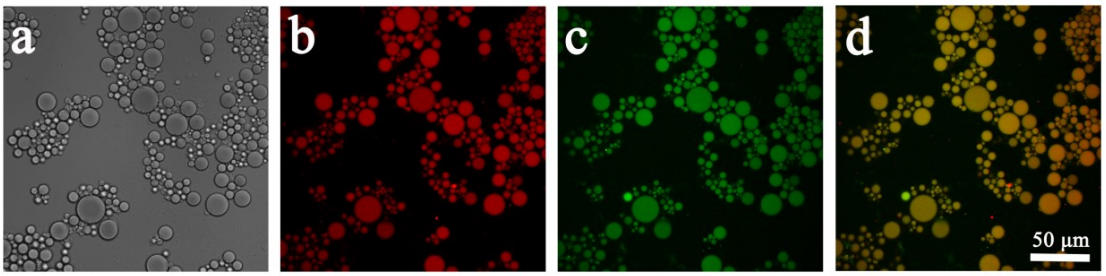

Fig. S23 Colocalization imaging of *Locusta migratoria* corpus adiposum incubated with **TPTIs** and BODIPY493/503 Green. a) Bright-field, b) red channel and c) green channel. d) merged images of panels (b) and (c). For **TPTIs**, λ_{ex}= 488 nm, λ_{em}= 600–750 nm; For BODIPY 493/503, λ_{ex}= 488 nm, λ_{em}= 500–570 nm. Concentrations: **TPTIs** (1.0×10^{-6} M), BODIPY493/503 Green (1×10^{-6} M).

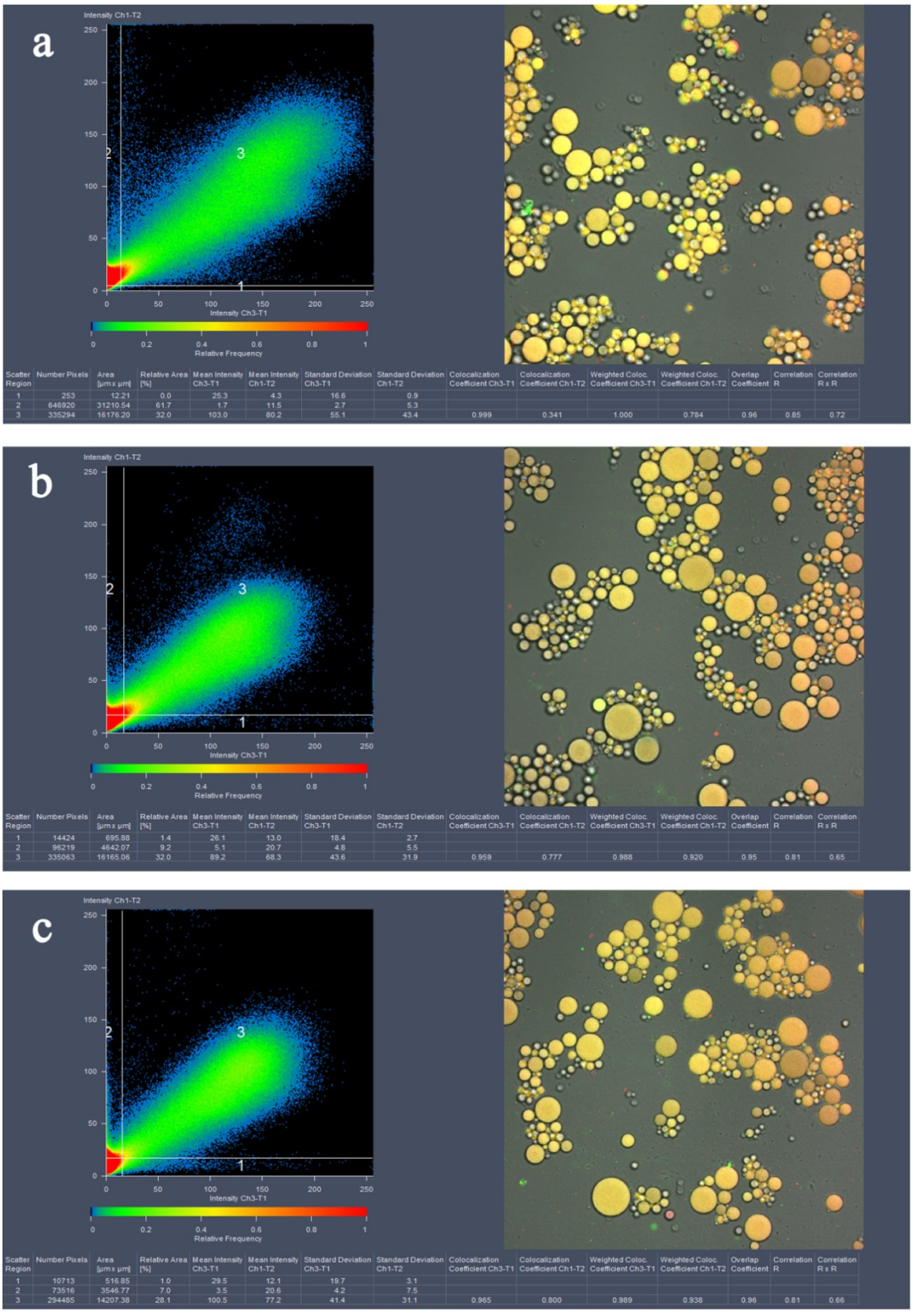

Fig. S24 Scatter plot of each AIEgen (a) **TPBIs**, (b) **TPFIs**, (c) **TPTIs** and BODIPY493/503 Green in *Locusta migratoria* corpus adiposum. Pearson correlation coefficients Rr = 0.96 (**TPBIs**), 0.95 (**TPFIs**) and 0.96 (**TPTIs**).

9. Colocalization imaging of *Caenorhabditis elegans*

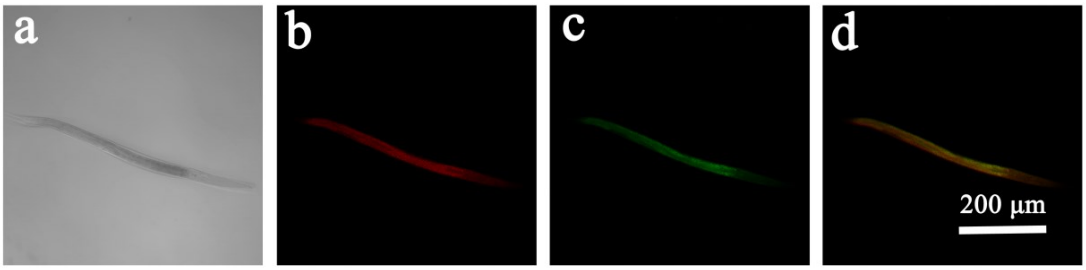

Fig. S25 Colocalization imaging of *Caenorhabditis elegans* incubated with **TPFIs** and BODIPY493/503 Green. a) Bright-field, b) red channel and c) green channel. d) merged images of panels (b) and (c). For **TPFIs**, λ_{ex}= 488 nm, λ_{em}= 600–750 nm; For BODIPY 493/503, λ_{ex}= 488 nm, λem= 500–570 nm. Concentrations: **TPFIs** (1 × 10^{-6} M), BODIPY493/503 Green (1.0 × 10^{-6} M).

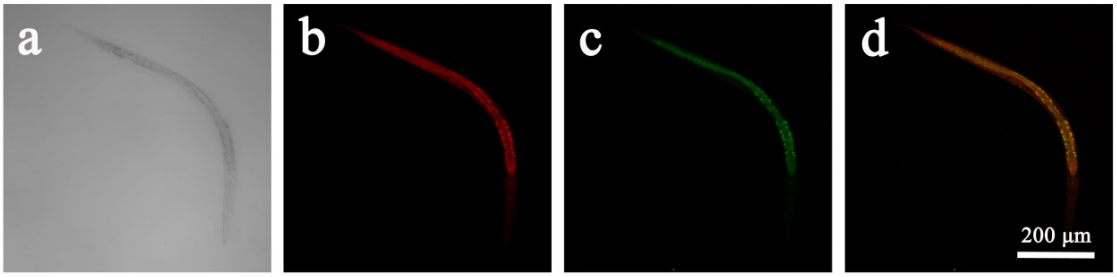

Fig. S26 Colocalization imaging of *Caenorhabditis elegans* incubated with **TPTIs** and BODIPY493/503 Green. a) Bright-field, b) red channel and c) green channel. d) merged images of panels (b) and (c). For **TPTIs**, λ_{ex}= 488 nm, λ_{em}= 600–750 nm; For BODIPY 493/503, λ_{ex}= 488 nm, λ_{em}= 500–570 nm. Concentrations: **TPTIs** (1 × 10^{-6} M), BODIPY493/503 Green (1.0 × 10^{-6} M).

10. Colocalization imaging of zebrafish

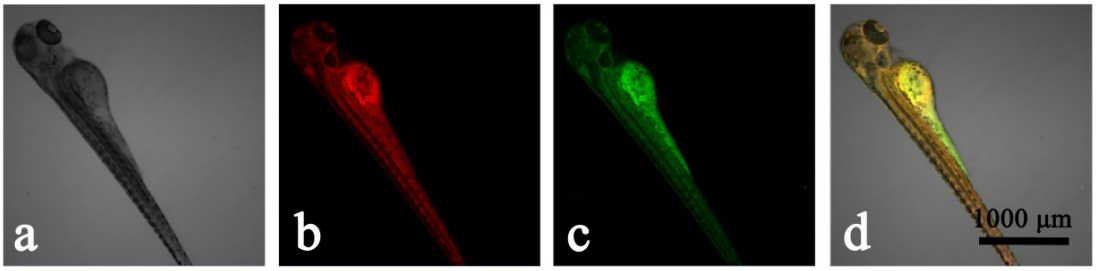

Fig. S27 Colocalization imaging of zebrafish incubated with **TPFIs** and BODIPY493/503 Green. a) Bright-field, b) red channel and c) green channel. d) merged images of panels (b) and (c). For **TPFIs**, λ_{ex}= 488 nm, λ_{em}= 600–750 nm; For BODIPY 493/503, λ_{ex}= 488 nm, λ_{em}= 500–570 nm. Concentrations: **TPFIs** (1 × 10^{-6} M), BODIPY493/503 Green (1.0 × 10^{-6} M).

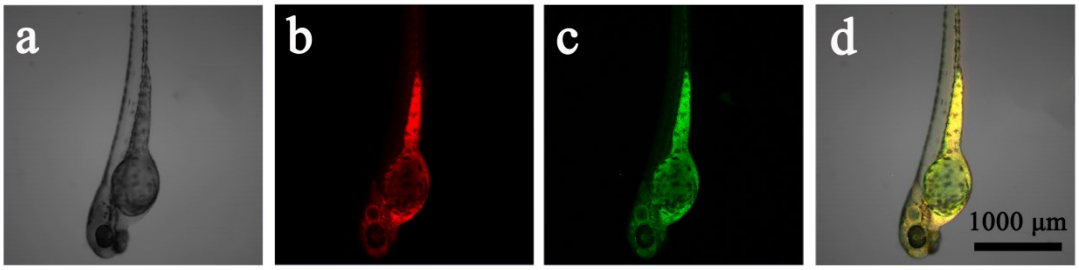

Fig. S28 Colocalization imaging of zebrafish incubated with **TPTIs** and BODIPY493/503 Green. a) Bright-field, b) red channel and c) green channel. d) merged images of panels (b) and (c). For **TPTIs**, λ_{ex}= 488 nm, λ_{em}= 600–750 nm; For BODIPY 493/503, λ_{ex}= 488 nm, λ_{em}= 500–570 nm. Concentrations: **TPTIs** (1 × 10^{-6} M), BODIPY493/503 Green (1 .0× 10^{-6} M).

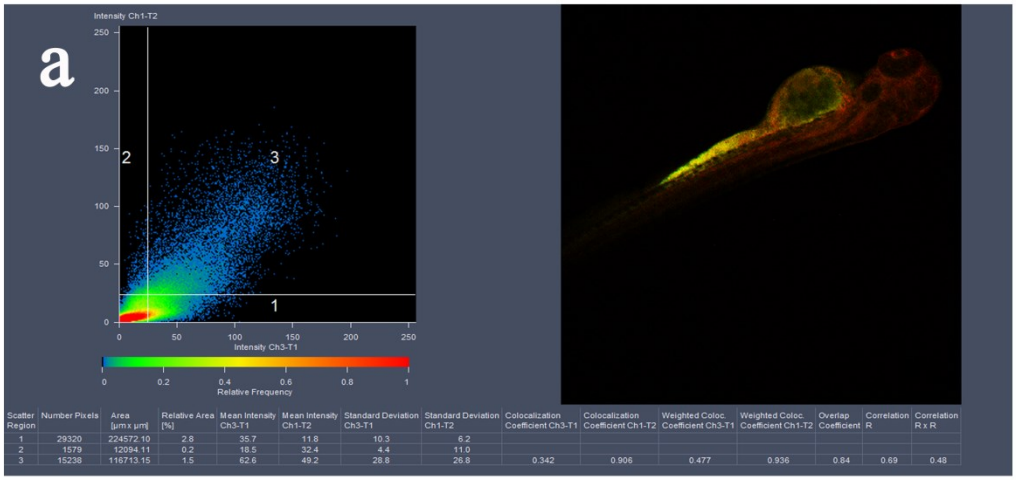

Scatter Region	Number Pixels	Area [µm x µm]	Relative Area [%]	Mean Intensity Ch3-T1	Mean Intensity Ch1-T2	Standard Deviation Ch3-T1	Standard Deviation Ch1-T2	Colocalization Coefficient Ch3-T1	Colocalization Coefficient Ch1-T2	Weighted Coloc. Coefficient Ch3-T1	Weighted Coloc. Coefficient Ch1-T2	Overlap Coefficient	Correlation R	Correlation R x R
1	29320	224572.10	2.8	35.7	11.8	10.3	6.2							
2	1579	12094.11	0.2	18.5	32.4	4.4	11.0							
3	15238	116713.15	1.5	62.6	49.2	28.8	26.8	0.342	0.906	0.477	0.936	0.84	0.69	0.48

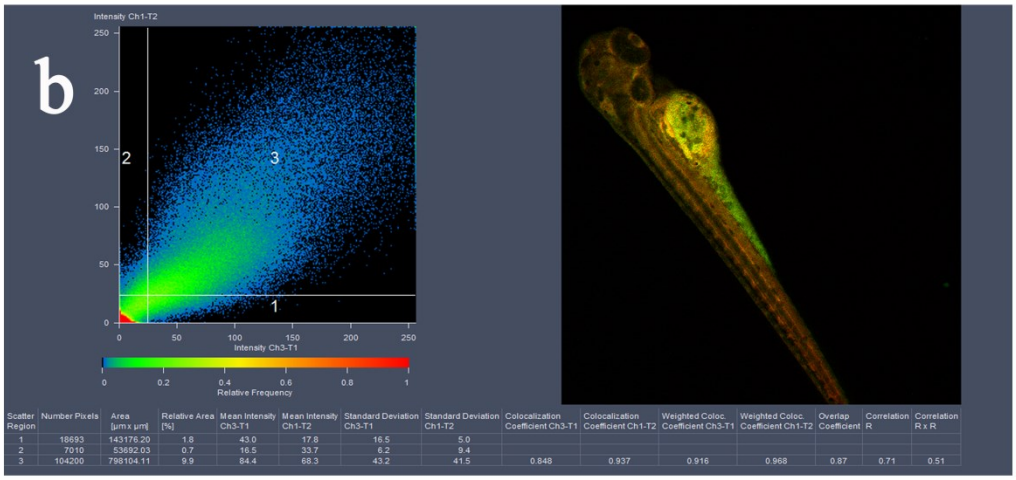

Scatter Region	Number Pixels	Area [µm x µm]	Relative Area [%]	Mean Intensity Ch3-T1	Mean Intensity Ch1-T2	Standard Deviation Ch3-T1	Standard Deviation Ch1-T2	Colocalization Coefficient Ch3-T1	Colocalization Coefficient Ch1-T2	Weighted Coloc. Coefficient Ch3-T1	Weighted Coloc. Coefficient Ch1-T2	Overlap Coefficient	Correlation R	Correlation R x R
1	18693	143176.20	1.8	43.0	17.8	16.5	5.0							
2	7010	53682.03	0.7	16.5	33.7	6.2	9.4							
3	104200	798104.11	9.9	84.4	68.3	43.2	41.5	0.848	0.937	0.916	0.968	0.87	0.71	0.51

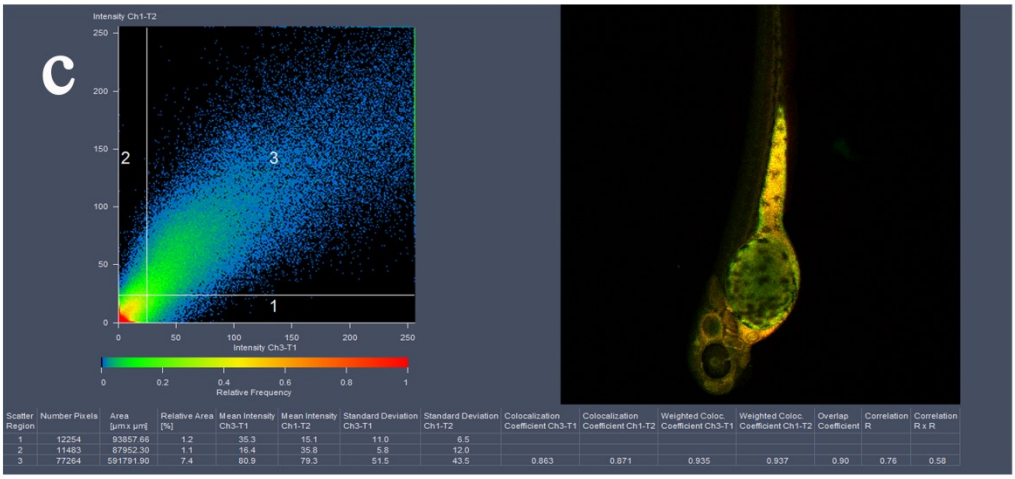

Scatter Region	Number Pixels	Area [µm x µm]	Relative Area [%]	Mean Intensity Ch3-T1	Mean Intensity Ch1-T2	Standard Deviation Ch3-T1	Standard Deviation Ch1-T2	Colocalization Coefficient Ch3-T1	Colocalization Coefficient Ch1-T2	Weighted Coloc. Coefficient Ch3-T1	Weighted Coloc. Coefficient Ch1-T2	Overlap Coefficient	Correlation R	Correlation R x R
1	12254	93857.66	1.2	35.3	15.1	11.0	6.5							
2	11483	87952.30	1.1	16.4	35.8	5.8	12.0							
3	77264	591791.90	7.4	80.9	79.3	51.5	43.5	0.863	0.871	0.935	0.937	0.90	0.76	0.58

Fig. S29 Scatter plot of each AIEgen (a) **TPBIs**, (b) **TPFIs**, (c) **TPTIs** and BODIPY493/503 Green in zebrafish. Pearson correlation coefficients Rr = 0.84 (**TPBIs**), 0.87 (**TPFIs**) and 0.90 (**TPTIs**).

11. Colocalization imaging of sunflower

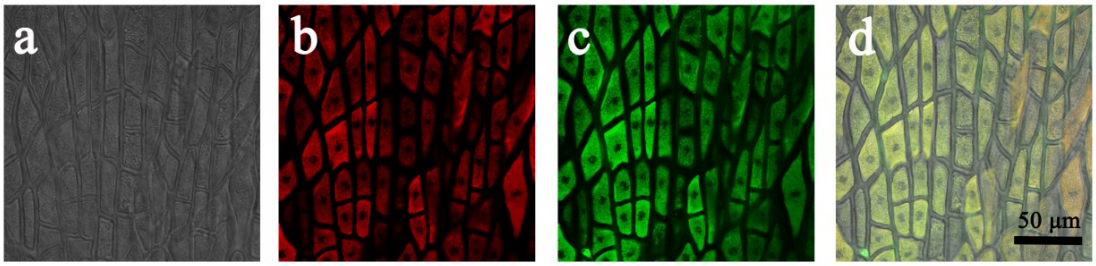

Fig. S30 Colocalization imaging of sunflower seed coat incubated with **TPFIs** and BODIPY493/503 Green. a) Bright-field, b) red channel and c) green channel. d) merged images of panels (b) and (c). For **TPFIs**, λ_{ex}= 488 nm, λ_{em}= 600–750 nm; For BODIPY 493/503, λ_{ex}= 488 nm, λ_{em}= 500–570 nm. Concentrations: **TPFIs** (1 × 10^{-6} M), BODIPY493/503 Green (1.0 × 10^{-6} M).

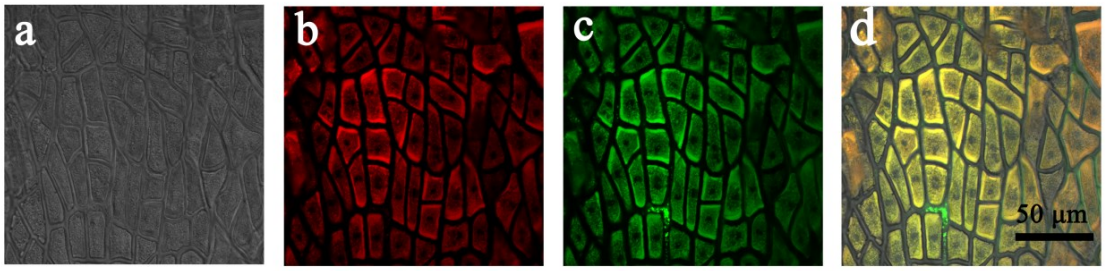

Fig. S31 Colocalization imaging of sunflower seed coat incubated with **TPTIs** and BODIPY493/503 Green. a) Bright-field, b) red channel and c) green channel. d) merged images of panels (b) and (c). For **TPTIs**, λ_{ex}= 488 nm, λ_{em}= 600–750 nm; For BODIPY 493/503, λ_{ex}= 488 nm, λ_{em}= 500–570 nm. Concentrations: **TPTIs** (1 × 10^{-6} M), BODIPY493/503 Green (1.0 × 10^{-6} M).

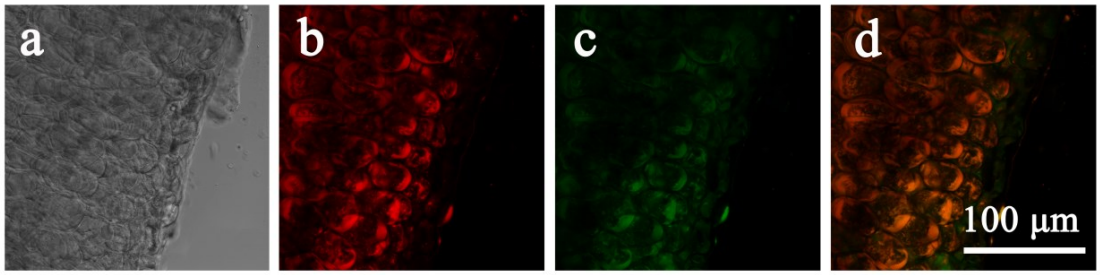

Fig. S32 Colocalization imaging of sunflower seed in section **a** incubated with **TPFIs** and BODIPY493/503 Green. a) Bright-field, b) red channel and c) green channel. d) merged images of panels (b) and (c). For **TPFIs**, λ_{ex}= 488 nm, λ_{em}= 600–750 nm; For BODIPY 493/503, λ_{ex}= 488 nm, λ_{em}= 500–570 nm. Concentrations: **TPFIs** (1 × 10^{-6} M), BODIPY493/503 Green (1.0 × 10^{-6} M).

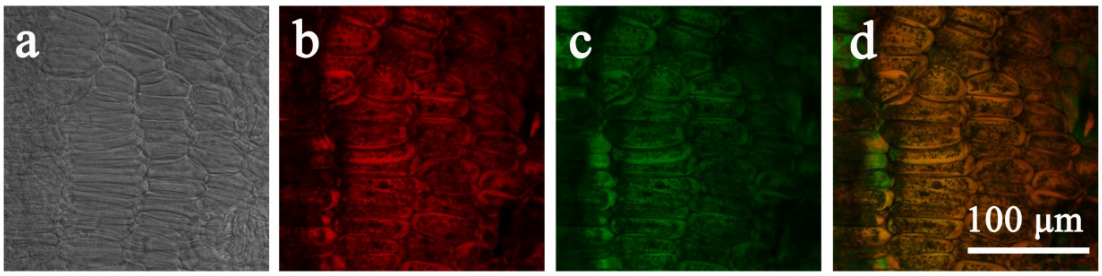

Fig. S33 Colocalization imaging of sunflower seed in section **b** incubated with **TPFIs** and BODIPY493/503 Green. a) Bright-field, b) red channel and c) green channel. d) merged images of panels (b) and (c). For **TPFIs**, λ_{ex}= 488 nm, λ_{em}= 600–750 nm; For BODIPY 493/503, λ_{ex}= 488 nm, λ_{em}= 500–570 nm. Concentrations: **TPFIs** (1 × 10^{-6} M), BODIPY493/503 Green (1.0 × 10^{-6} M).

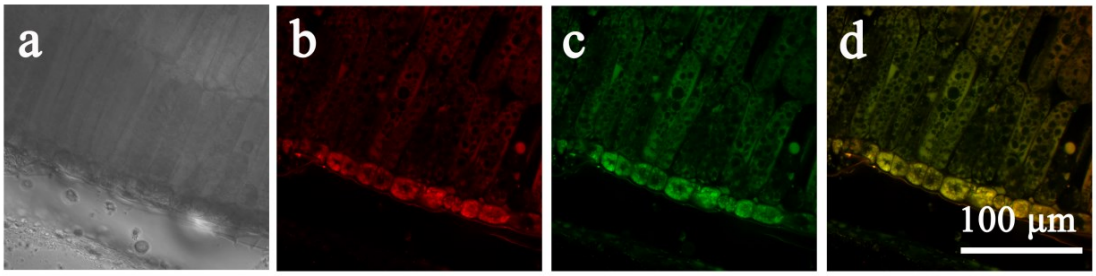

Fig. S34 Colocalization imaging of sunflower seed in section **c** incubated with **TPFIs** and BODIPY493/503 Green. a) Bright-field, b) red channel and c) green channel. d) merged images of panels (b) and (c). For **TPFIs**, λ_{ex}= 488 nm, λ_{em}= 600–750 nm; For BODIPY 493/503, λ_{ex}= 488 nm, λ_{em}= 500–570 nm. Concentrations: **TPFIs** (1 × 10^{-6} M), BODIPY493/503 Green (1.0 × 10^{-6} M).

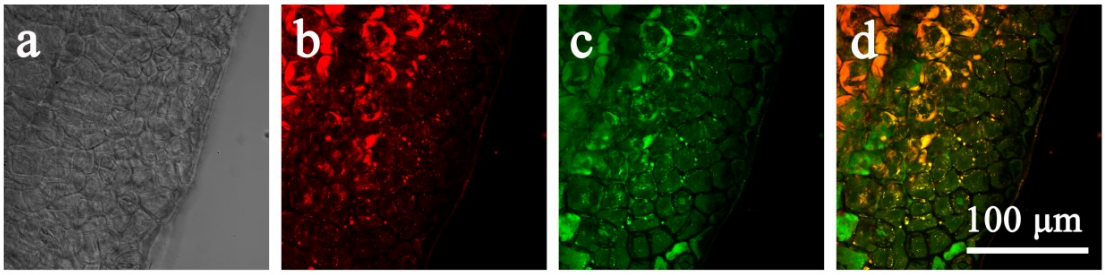

Fig. S35 Colocalization imaging of sunflower seed in section **a** incubated with **TPTIs** and BODIPY493/503 Green. a) Bright-field, b) red channel and c) green channel. d) merged images of panels (b) and (c). For **TPTIs**, λ_{ex}= 488 nm, λ_{em}= 600–750 nm; For BODIPY 493/503, λ_{ex}= 488 nm, λ_{em}= 500–570 nm. Concentrations: **TPTIs** (1 × 10^{-6} M), BODIPY493/503 Green (1.0 × 10^{-6} M).

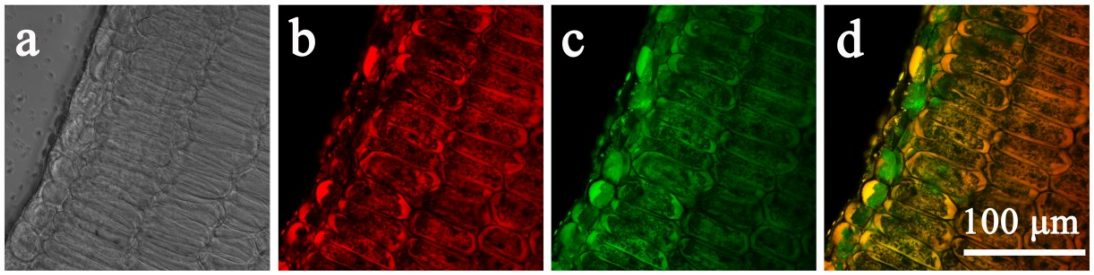

Fig. S36 Colocalization imaging of sunflower seed in section **b** incubated with **TPTIs** and BODIPY493/503 Green. a) Bright-field, b) red channel and c) green channel. d) merged images of panels (b) and (c). For **TPTIs**, λ_{ex}= 488 nm, λ_{em}= 600–750 nm; For BODIPY 493/503, λ_{ex}= 488 nm, λ_{em}= 500–570 nm. Concentrations: **TPTIs** (1 × 10^{-6} M), BODIPY493/503 Green (1.0 × 10^{-6} M).

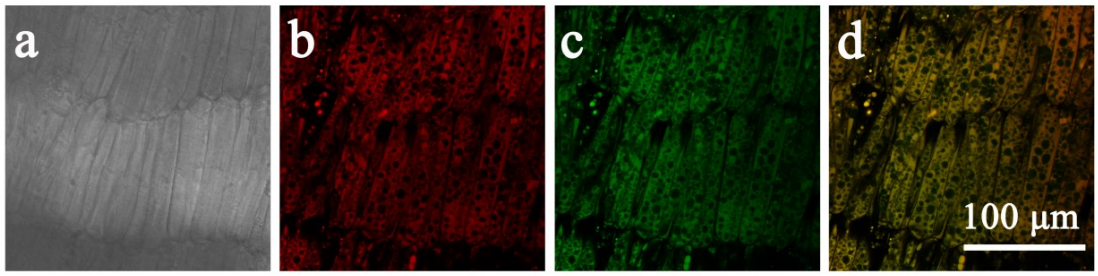

Fig. S37 Colocalization imaging of sunflower seed in section **c** incubated with **TPTIs** and BODIPY493/503 Green. a) Bright-field, b) red channel and c) green channel. d) merged images of panels (b) and (c). For **TPTIs**, λ_{ex}= 488 nm, λ_{em}= 600–750 nm; For BODIPY 493/503, λ_{ex}= 488 nm, λ_{em}= 500–570 nm. Concentrations: **TPTIs** (1 × 10^{-6} M), BODIPY493/503 Green (1.0 × 10^{-6} M).

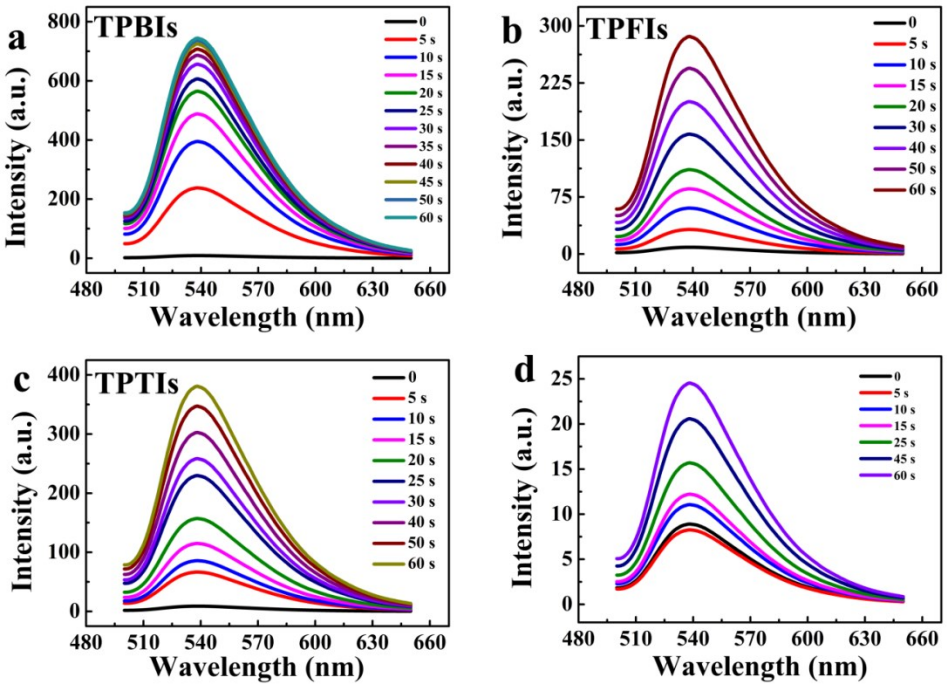

Fig. S38 The fluorescence spectra of three AIEgens (a, b, c) in the presence of DCF-DA and the DCF-DA alone (d) at different light times, excitation wavelength: 488 nm.

Table S1. Crystal data and structure refinement of **TPTIs**.

Identification code	**TPTIs**
Empirical formula	$C_{35}H_{29}N_3S$
Formula weight	523.21
Temperature / K	293(2)
Wavelength / Å	0.71073
Crystal system	triclinic
Space group	P-1
a / Å	8.2367(7)
b / Å	12.9715(11)
c / Å	14.0133(12)
α /°	86.405(4)
β /°	75.922(3)
γ / °	86.498(3)
Volume s/ Å^3	1447.8(2)
Z	2

Calculated density / mg / m^3	1.134
Absorption coefficient / mm^{-1}	0.137
F(000)	494
Crystal size / mm^3	0.2×0.15×0.13
Theta range for data collection / °	2.97 to 24.20
Limiting indices	-9≤h≤9, -14≤k≤14, -16≤l≤16
Reflections collected / unique	10150 / 4017 [R_{int} = 0.0477]
Completeness to theta = 24.20	86.2 %
Absorption correction	None
Refinement method	Full-matrix least-squares on F^2
Data / restraints / parameters	4017/0/355
Goodness-of-fit on F^2	1.196
Final R indices [I>2σ(I)]	R_1 = 0.1239, wR_2 = 0.2672
R indices (all data)	R_1 = 0.1603, wR_2 = 0.2849
Extinction coefficient	0.036(6)
Largest diff. peak and hole / e. $Å^{-3}$	0.417 and -0.396

Table S2. Data of bandgaps of theoretical study and cyclic voltammetry.

Compound	$E_{\text{oxd oneset}}$ V	E_{HOMO}	E_g^{opt} eV	E_{LUMO}	HOMO $^{\text{DFT}}$ eV	LUMO $^{\text{DFT}}$ eV	E_g $^{\text{DFT}}$ eV
TPBIs	0.82	-5.23	2.20	-3.03	-5.13	-2.82	2.31
TPFIs	0.75	-5.16	2.00	-3.16	-5.01	-2.74	2.27
TPTIs	0.76	-5.17	2.05	-3.12	-5.11	-2.81	2.30

E_{HOMO} = - e($E_{\text{oxd oneset}}$ + 4.41) V;

E_g^{opt} = h × f = h × $\frac{c}{\lambda_{a.e.}} \approx \frac{1240}{\lambda_{a.e.}}$;

$E_{\text{LUMO}} = E_{\text{HOMO}} + E_g^{opt}$.

Table S3. Photophysical properties of LDs probes and their applications.

Dye[ref]	$\lambda_{ex}/\lambda_{em}$, nm	ε, M^{-1}, cm^{-1}	Application
Nile Red [2]	553/635 (MeOH)	44,000	Cells
PyrPy 10d [3]	356/449 ($CHCl_3$)	12,400	Cells
PyrPy 11c	344/447 ($CHCl_3$)	13,200	Cells
AF8 [4]	380/479 (DMSO)	n.r.	Cells
AFN	428/592 (DMSO)	n.r.	Cells
AF10	356/477 (DMSO)	n.r.	Cells
NAP-Ph [5]	409/523 (water)	n.r.	imaging in cells and tissues
NAP-Br	409/525 (water)	n.r.	imaging in cells and tissues
NAP-CF_3	425/560 (water)	n.r.	imaging in cells and tissues
NAP-Py	413/541 (water)	n.r.	imaging in cells and tissues
Phos 2a [6]	439/554 (DMSO)	n.r.	Cells
Phos 3a	429/512 (DMSO)	n.r.	Cells
Phos 2b	437/554 (DMSO)	n.r.	Not applicable for cells
Phos 3b	374/550 (DMSO)	n.r.	Not applicable for cells
FAS [7]	322/600 (water)	n.r.	Cells
DPAS	301/550 (water)	n.r.	Cells
BTD-Lip [8]	455/624 (MeCN)	7586	Cells and worms
TPMN [9]	441/637 (solid)	n.r.	Cells, zebrafish imaging and therapy
TTMN	483/672 (solid)	n.r.	Cells, zebrafish imaging and therapy
MeTTMN	441/681 (solid)	n.r.	Cells, zebrafish imaging and therapy
MeOTTMN	499/701(solid)	n.r.	Cells, zebrafish imaging and therapy
DCMa [10]	478/665 (water)	n.r.	1PE and 2PE imaging in cells
DCIs	510/709 (water)	n.r.	1PE and 2PE imaging in cells
DCFu	538/755 (water)	n.r.	1PE and 2PE imaging in cells
SMCy3 [11]	528/550 (toluene)	94,000	Cells and tissue imaging
SMCy3.5	551/572 (toluene)	124,000	Cells and tissue imaging
SMCy5	615/642 (toluene)	203,000	Cells and tissue imaging
SMCy5.5	634/661 (toluene)	168,000	Cells and tissue imaging
SMCy7	683/721 (toluene)	109,000	Cells and tissue imaging
SMCy7.5	705/746 (toluene)	89,000	Cells and tissue imaging
PEG-NBD[12]	470/521 (toluene)	n.r.	discrimination living and dead cells
TPA-SD [13]	400/550 (water)	n.r.	diagnosis diseases related to LDs
DPFB-NMe_2 [14]	435/578 (DMSO)	n.r.	Cells and zebrafish
TTNIR [15]	512/724 (ACN)	n.r.	cellular imaging and therapy
TPBIs (this work)	494/666 (toluene)	22,800	Cells, excised adipose tissues, zebrafish, *Caenorhabditis elegans*, sunflower kernels imaging and therapy
TPFIs (this work)	549/683 (toluene)	43,900	Cells, excised adipose tissues, zebrafish, *Caenorhabditis elegans*, sunflower kernels imaging and therapy
TPTIs (this work)	547/684 (toluene)	32,800	Cells, excised adipose tissues, zebrafish, *Caenorhabditis elegans*, sunflower kernels imaging and therapy

References

1 Y. Li, T. Ren and W. J. Dong, J. Photochem, *Photobiol*., 2013, **251**, 1–9.

2 P. Greenspan, E. P. Mayer, S. D. Fowler, *J. Cell Biol*., 1985, **100**, 965–973.

3 E. Wang, E. Zhao, Y. Hong, J. W. Y. Lam and B. Z. Tang, *J. Mater. Chem. B*, 2014, **2**, 2013–2019.

4 A. Sharma, S. Umar, P. Kar, K. Singh, M. Sachdev and A. Goel, *Analyst*, 2016, **141**, 137–143.

5 G. Niu, R. Zhang, J. P. C. Kwong, J. W. Y. Lam, C. Chen, J. Wang, Y. Chen, X. Feng, R. T. K. Kwok, H. H. Y. Sung, I. D. Williams, M. R. J. Elsegood, J. Qu, C. Ma, K. S. Wong, X. Yu and B. Z. Tang, *Chem. Mater.*, 2018, **30**, 4778–4787.

6 E. Öberg, H. Appelqvist and K. P. R. Nilsson, *Front. Chem.*, 2017, **5**.

7 Z. Wang, C. Gui, E. Zhao, J. Wang, X. Li, A. Qin, Z. Zhao, Z. Yu and B. Z. Tang, *ACS Appl. Mater. Interfaces*, 2016, **8**, 10193–10200.

8 A. A. R. Mota, J. R. Correa, L. P. de Andrade, J. A. F. Assumpção, G. A. de Souza Cintra, L. H. Freitas-Junior, W. A. da Silva, H. C. B. de Oliveira and B. A. D. Neto, *ACS Omega*, 2018, **3**, 3874–3881.

9 D. Wang, H. Su, R. T. K. Kwok, G. Shan, A. C. S. Leung, M. M. S. Lee, H. H. Y. Sung, I. D. Williams, J. W. Y. Lam and B. Z. Tang, *Adv. Funct. Mater.*, 2017, **27**, 1704039.

10 Z. Zheng, T. Zhang, H. Liu, Y. Chen, R. T. K. Kwok, C. Ma, P. Zhang, H. H. Y. Sung, I. D. Williams, J. W. Y. Lam, K. S. Wong and B. Z. Tang, *ACS Nano.*, 2018, **12**, 8145–8159.

11 M. Collot, T. K. Fam, P. Ashokkumar, O. Faklaris, T. Galli, L. Danglot and A. S. Klymchenko, *J. Am. Chem. Soc.*, 2018, **140**, 5401–5411.

12 F. Yu, X. Jing and W. Lin, *Sens. Actuators, B*, 2020, **302**, 127207.

13 J. Shi, Y. Tian, B. Guo, Y. Wu, J. Jing, R. Zhang and X. Zhang, *Sens. Actuators, B*, 2019, **284**, 545–552.

14 N. Zhao, C. Ma, W. Yang, W. Yin, J. Wei and N. Li, *Chem. Commun.*, 2019, **55**, 8494–8497.

15 W. Xu, M. M. S. Lee, Z. Zhang, H. H. Y. Sung, I. D. Williams, R. T. K. Kwok, J. W. Y. Lam, D. Wang and B. Z. Tang, *Chem. Sci.*, 2019, **10**, 3494–3501.